PAPER REF: 7197

ADVANCED NDT PROCEDURES AND THERMAL DATA PROCESSING ON CFRP AERONAUTICAL COMPONENTS

V. Dattoma, R. Nobile, F.W. Panella[(*)], A. Pirinu, A. Saponaro

Department of Engineering for Innovation, University of Salento, Lecce, Italy
[(*)]*Email:* francesco.panella@unisalento.it

ABSTRACT

In this work, active Pulsed Thermography (PT) was used to improve CFRP aeronautical parts investigation in order to detect sub-surface defects. Composite materials are prone to successful thermal/infrared NDT analyses, since defects are easily characterised by their surface 'footprints' under thermal pulses with reliable results. Better defect characterisation is achieved analysing data with better data processing and procedures, providing detailed contrasts maps where defects' edges are distinguished. Thermal data are analysed for different specimens with artificial defects and experimental procedures are verified on real a failure in structural aeronautical component. Finally, improved data processing allowed better identifying the damaged areas on specimens.

Keywords: aeronautical component, CFRP, NDT, pulsed thermography, standard defects, thermal contrast.

INTRODUCTION

Material defects are the major sources of composite failures. The defects in FRP composite Structures could be divided in manufacturing defects (delamination, voids, porosity, micro cracking, etc.) and in-service defects (impact or fatigue damage, Cracks, Debonding, Delamination, Erosion, etc.). In general, a combination of different and contemporaneous voids, matrix cracks, and multiple delaminations is present. Structural integrity is a formalized process that uses advanced non-destructive testing (NDT) methods in order to detect, localize and determine the damage risk (Gholizadeh, 2016).

Thermal methods are most effective for thin laminates or for defects near the surface. We can adopt the passive or the active approach (Czichos, 2013). Active thermographic techniques include Pulse thermography (PT), which consists of rapidly heating the specimen and then recording its temperature decay curve and in authors' opinion is still a valid an robust technique. The free-defect areas conduct heat more efficiently than defective areas and the amount of heat that is either absorbed or reflected indicates the quality state of the inspected area (Dattoma *et al*., 2017).

MATERIALS AND METHODS

CFRP components

For the optimization and the calibration of better signal algorithm processing, standard specimens with artificial defects, built with expanded polystyrene inserts, are used; these are crucial to determine the threshold detectability limits of the proposed technique in an

improved way (Carofalo *et al*. 2014): defect size, depth, and type in order to certify the inspections.

The CFRP specimens are aeronautical production plates assembled to englobe artificial defects: two plates with different thicknesses were realized by bonding of two square laminates (120.7 x 120.7 mm2) with a central hole according to the constructive drawing (Figure 1). The plates of different thicknesses are glued together and expanded polystyrene defects are inserted between plates in order to simulate delaminations. The different sizes of defects allow us evaluating the influence of their size, depth (different if measured from the opposite sides) and thickness for a possible and reliable detection (A. P. Carofalo *et al*., 2014).
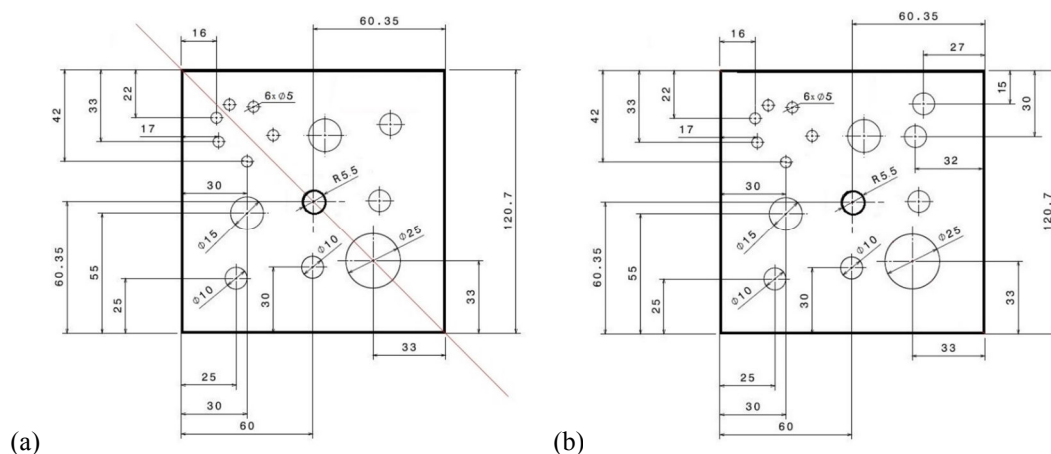

Fig. 1 - Drawing of artificial defects position on the plate I (a) and on the plate II (b).

Furthermore, the defects have different sizes to evaluate the influence of dimension, depth and thickness on their detection possibility. The original laminate plates are with symmetric lamina oriented ±0/90°, coupled with ±45°at borders with different thicknesses (A. P. Carofalo *et al*., 2014). The polymeric disks were glued individually or in pairs in order to create a thickness of 0.6 mm and 1.2 mm respectively. In both specimens (Figure 2), the defects can be observed at two different depths from external surfaces. In particular, in the plate-I, the thickness of the laminates are 4.9 mm (side A or 14 layers) and 2.8 mm (side B or 8 layers), for a total of 7.7 mm. Instead, in the plate-II, the thicknesses of the single laminates are respectively 2.1 mm (side A or 6 layers) and 2.8 mm (side B or 8 layers) for a total of 4.9 mm.
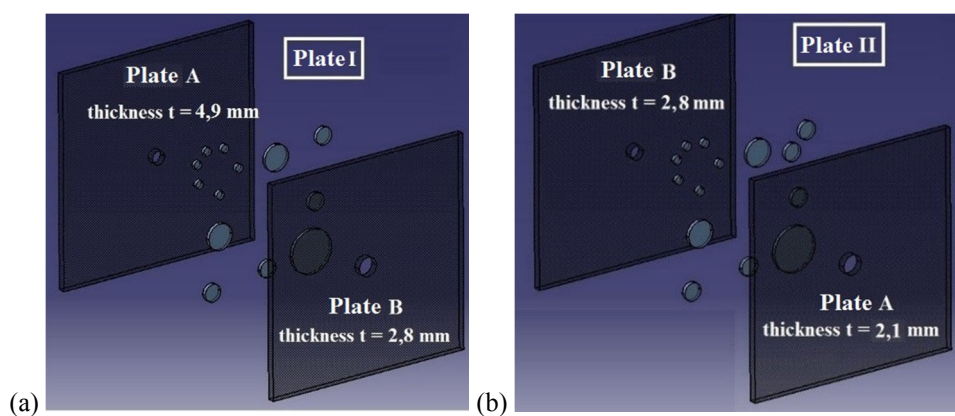

Fig. 2 - Structure of the plate-I (a) and of the plate II (b).

The plate I allows to analyze defects of elevate depth. Defects with different sizes are created to study the relationship between the detection of a defect according to its size and depth together. The aim of lower specimen thickness is to verify the possibility to analyze artificial defects of the same nature but with a smaller diameter. For this reason, the side-A of the plate-II is covered with non-shiny black paint to eliminate reflection problems. This solution is useful because the 5 mm diameter defects are inspected with particular care on that side of the specimen. The information in terms of thermal conductivity and density of the CFRP constituents are shown in Table 1. The resin is an epoxy resin EC 130 LV and the hardener W340 with ratio 100:37 (produced by Altana Varnish Compounds).

Table 1 - Mechanical properties of carbon fibre and epoxy resin of plates' material.

Material	Density [g/cm^3]	Young modulus [Mpa]	Ultimate stress [Mpa]	Areal weight [g/m^2]	Thermal conductivity coef. [W/mK]	Ultimate strain [%]
Carbon fiber	1.65	/	/	240	~15	/
Epoxy resin	1,14÷1,16	2900÷3100	75÷80	0.1919	~0,22	8,5÷9

Table 2 - Artificial defect's geometry in the plates.

Defect	1	2	3	4	5	6	7
N. Defect in plate-I	1	2	1	3	2	1	3
N. Defect in plate-II	1	4	1	3	1	1	3
Diameter [mm]	25	10	15	5	10	15	5
Thickness[mm]	0,6	0,6	0,6	0,6	1,2	1,2	1,2

In addition, an aeronautical multi-stringer component of medium size (Dim. 914.4 x 762 mm^2) in carbon fibre laminates is studied; Figure 3(a) shows the geometry of the structural multi-stringer component. All laminates are CFRP laminates with different ply layers (Table 3). In this component, rivets secure the ribs on the skin. The component presents an artificial discontinuity in the form of a large cut (Dim. 152.4 x 6.35 mm^2) with extremities. This artificial damage on the skin interrupts the central stringer and simulates the presence of impact damage on the stringers 'area (Figure. 1 (b)). The information in terms of material and lamina properties constituents are shown in Table 3.
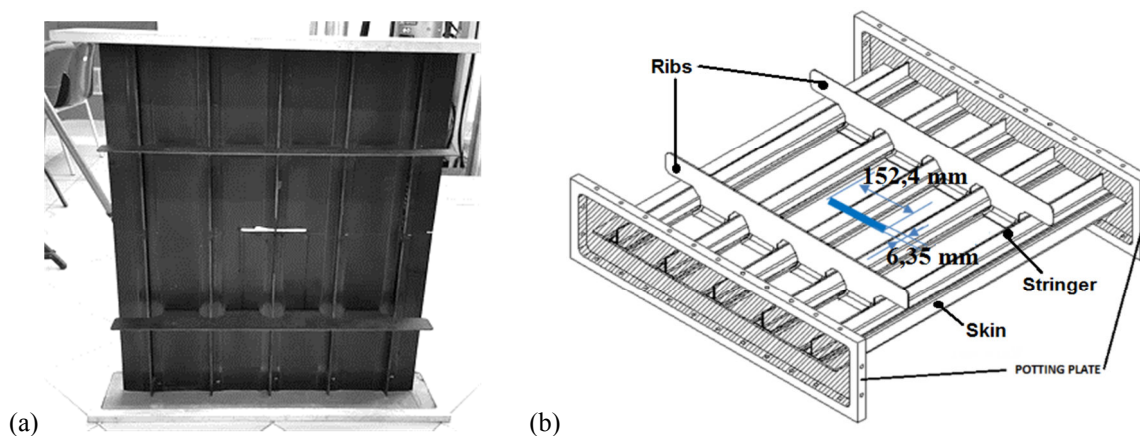

(a)   (b)

Fig. 3 - CFRP multi stringer multi-stringer component's geometry (a) and artificial damage's geometry (b).

Table 3 - Properties of composite parts of multi-stringer component.

Part component	Sub-Part component	Material	Lamina Thickness [mm]	N° plies	layup
Skin	Skin Thin	IMS/977-2	0,186	20	[45/90/-45/-45/45/90/0/-45/45/0]$_S$
	Skin Big	IMS/977-2	0,186	24	[45/90/0/0/-45/-45/45/90/0/-45/45/0]$_S$
Stringer		IMS/977-2	0,186	12	[45/90/0/0/-45/0]$_S$
Rib		HTA/977-2	0,208	12	[45/0/-45/90/45/0]$_S$

Experimental setup and inspection methods

Thermographic tests have been conducted in the Experimental Laboratory located in the Engineering Faculty of the University of Salento. Thermographic set-up means both the equipment used to test and the appropriate arrangement to carry out the test, proved influent in results.

The equipment used to conduct thermographic tests consists of an array of four halogen lamps, each of 1000 W that generate the light signal, a wave generator (which controls the various excitation sources), SC7700 model 7500M thermal camera of FLIR Advanced Thermal Solutions (Detector Materials In-Sb, 320×256 pixels) and custom processing software.

In thermal tests, the CFRP plate's surface is positioned at a distance of 0.5 m from lamps. Figure 4 show the best lay-up of the thermographic setup that will be used for all the tests.
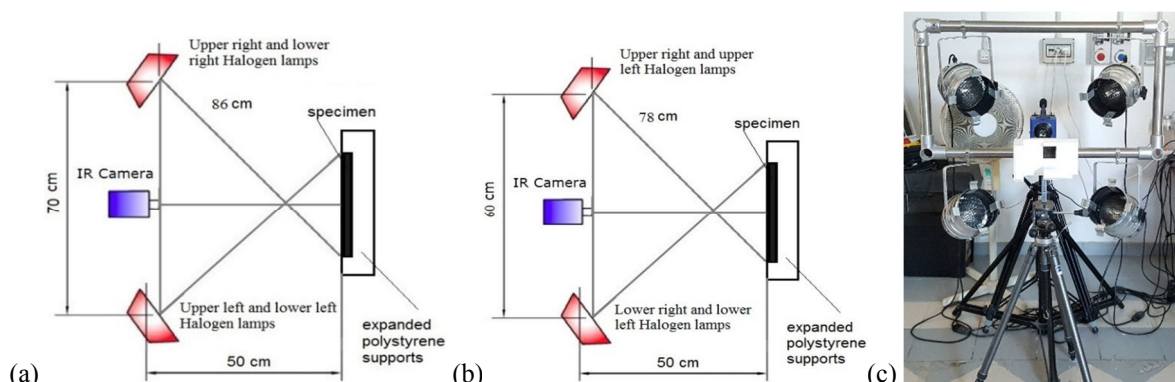

Fig. 4 - Top view (a) and lateral view (b) of the thermographic setup for CFRP plates' acquisition and experimental setup (c).

Employing this set-up, optimized to obtain an optional uniform heating of the exposed surface, twelve total tests are conducted: six on the plate-I (three for both sides) and six on the plate-II (three for both sides), by selecting different heating times (Table 4).

Table 4 - Scheduling tests for the investigations with different heat pulses.

Specimen	N° Test	Frame rate [Hz]	Acquisition time [s]	Heating time [s]	Total frames
CFRP plate-I on side B and plate-II on both sides	1	5	200	12	1000
	2	5	200	15	1000
	3	5	250	20	1250
CFRP plate-I on side A	1	5	100	20	500
	2	5	100	30	500
	3	5	100	40	500

For the multi-stringer real component, the surface is positioned at a distance of 0.72 m from the four Halogen lamps 1000 W. Figure 5 shows the lay-up of the thermographic setup that will be used for all the tests described in the case of large computed inspection.
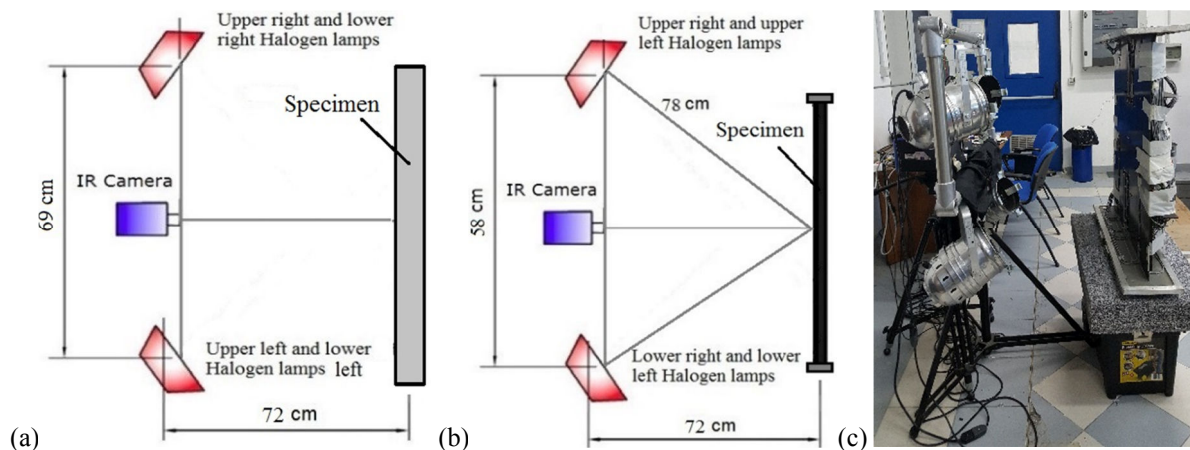

Fig. 5 - Top view (a) and lateral view (b) of the thermographic setup for multi-stringer component's acquisition.

Employing this set-up, performing tests of thermography pulsed on CFRP multi-stringer component, to obtain a uniform heating of the exposed surface (central zone), five total tests are conducted, by selecting different times heating (Table 5).

Table 5 - Scheduling tests for the multi-stringer component's investigation

Specimen	N° Test	Frame rate [Hz]	Acquisition time [s]	Heating time [s]	Total frames
CFRP aeronautical multi-stringer component	1	5	30	3	150
	2	5	60	7	300
	3	5	50	10	250
	4	5	120	15	600
	5	5	70	20	350

Thermal contrast results

The thermal contrast is basic parameter for defect localization by means of Pulsed Thermal NDT. The surface temperature contrast is used to investigate the defect detectability, using pulsed transient thermography (Dattoma *et al*., 2012).

A preliminary algorithm can be implemented in the MATLAB environment, to upload the 3-dimensional matrix of thermal frames and to return selected thermal maps of specimen for various tests, highlighting in particular various heat accumulation sites obtained over time, between free-defect areas (intact zones), and damaged areas (Dattoma *et al*., 2017). The absolute contrast CA is defined by the equations (1).

$$C_A(t) = T_{DZ}(t) - T_{IZ}(t) \tag{1}$$

Where the two term are the mean temperature in the reference area and the 'DZ' and 'IZ' refer to the defective and intact zones at given time (t) during the cooling transient phase. Absolute contrast method has limitations due to the used set-up and the operator choice of ideal areas for the contrast computation test. Therefore, the main drawback of classical thermal contrast analysis is establishing an arbitrary intact zone for each selected defect, especially if automated investigation is needed. Even when undamaged zone definition is straightforward, considerable variations of results are observed with the location choice of free-defect zone (Dattoma *et al*., 2017) and also with the dimension choice of the identified damaged window.

The Source Distribution Image (SDI) is generally used for selecting a free-defects portion of the specimen that presumably receives the same thermal flow of the corresponding damaged area (Boras *et al*., 2010).

In Figures 6 (a) and (b), the thermograms analysis at the beginning of the cooling phase allows us to estimate the heat distribution quality in terms of its uniformity, as well as the presence or absence of pre-accumulation of heat in the defective areas.
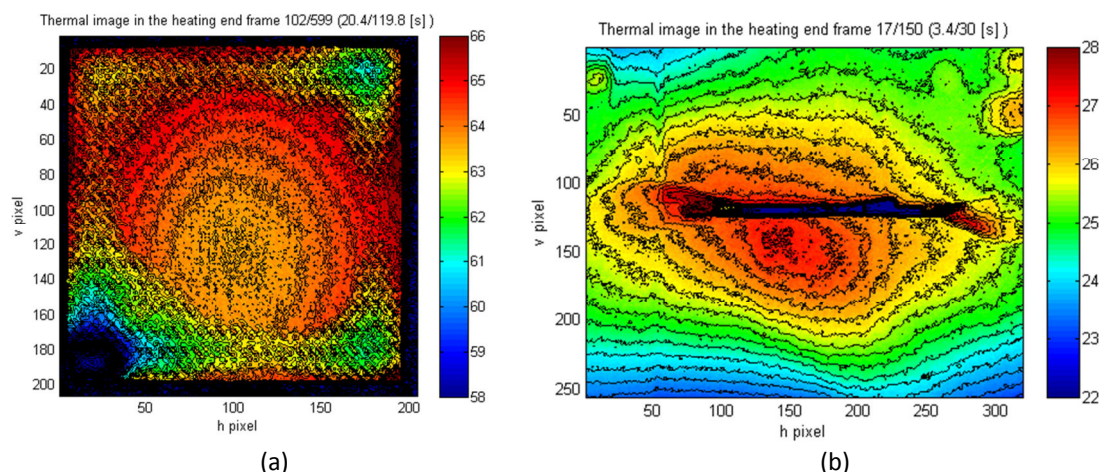

(a)

(b)

Fig. 6 - Maps of isotherms at the beginning of the cooling phase for artificial plate-I, side B (a) and for the damaged zone of real component (b) using respectively heating times of 20s and 3s.

The analysis of the isotherms from cooling thermograms shows the non-uniformity of heat deposition on the component; the used C_A algorithm takes into account the SDI method during the selection of the intact points, corresponding to the previously determined defective regions as indicated in Figure 7(a). Based on the principle of equal excitation energy, the SDI approach should minimize errors in absolute thermal contrast evaluation.

After choosing a thermal frame, where the defects are more distinguishable, the algorithm provides an interactive analysis procedure for selected defective and intact zones section. This procedure is automatically iterated many times for all defects; Figure 7 (a) shows a thermogram example of plate -I for processing a 25 mm diameter defect (dif_1), the 10 mm diameter defect (dif_2) and reference intact zone (int_1). In the same way On the central damage of the multi-stringer component, the thermogram of Figure 7(b) highlights the left (dif_1) and right (dif_2) damaged areas near the central cut and the reference intact area (int_1), since the component has been previously loaded under compression and damage has been accumulated around the artificial discontinuity.
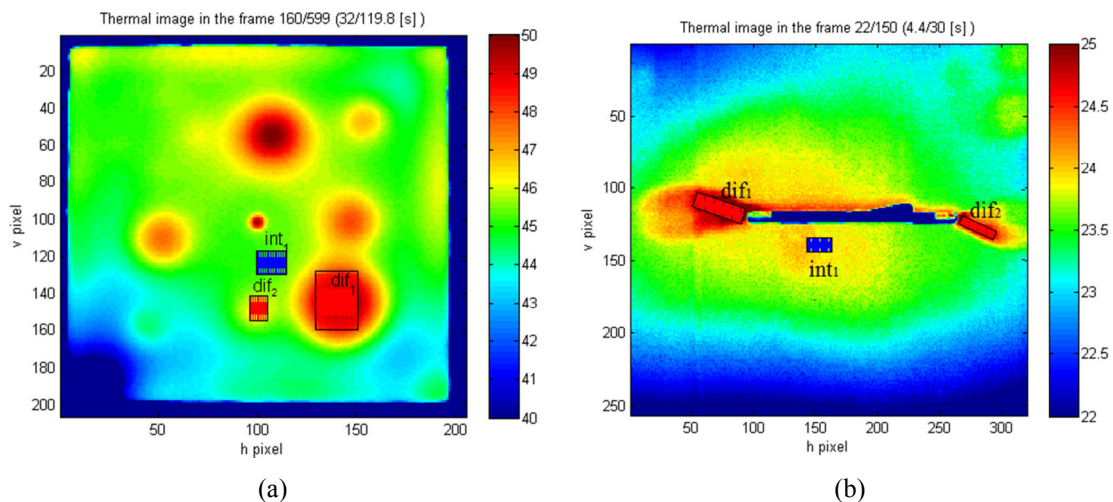
(a)　　　　　　　　　　　　　　　　(b)

Fig. 7 - Thermal image of plate-I obtained after 11.6 cooling seconds after heating pulse of 20s (a) and display of temperature for aeronautical component after 1 cooling seconds and heating pulse of 3s (b).

From temperatures acquired in the selected spots, the Matlab routine calculate the diagram of absolute contrasts, as calculated in the selected zones. The code provides diagrams of absolute contrast Ca during the time, defined in equation (1)

These diagrams allow for a more reliable comparison between the various damaged zones. Figure 8, 9, 10 and 11 show examples of typical thermal profiles in the intact zones and the defective area and the relative Absolute contrast trend.
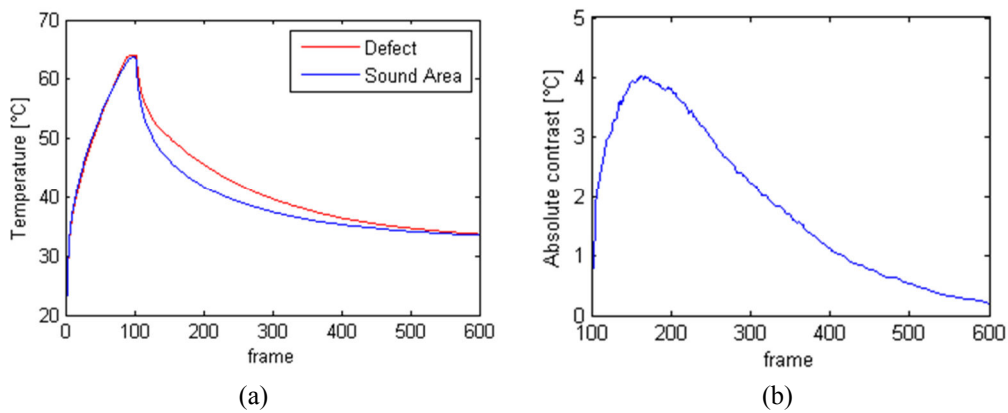

(a)　　　　　　　　　　　　　　　　(b)

Fig. 8 - Thermal profiles (a) and the Absolute contrast examples (b) for defect-1 (Ø 25 mm) and intact area (int_1) for plate-I.

(a)　　　　　　　　　　　　　　　　(b)
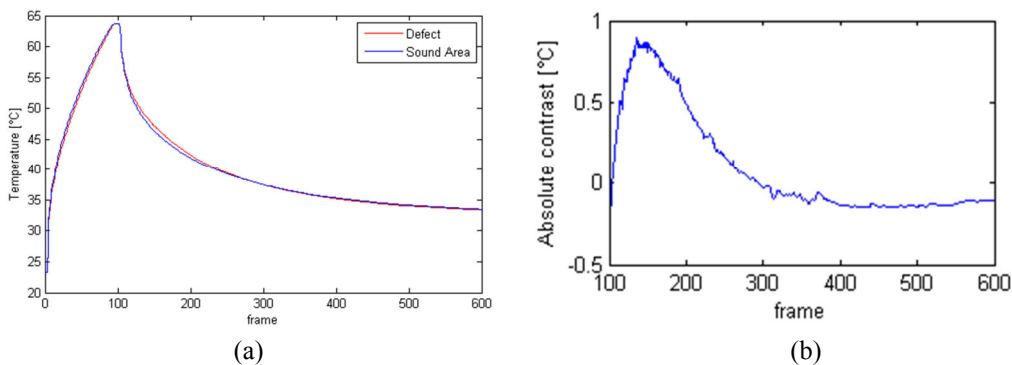
Fig. 9 - Thermal profiles (a) and the Absolute contrast examples (b) for defect-2 (Ø 10 mm) and intact zone for plate-I.

(a)　　　　　　　　　　　　　　　　(b)

Fig. 10 - Thermal profiles (a) and the Absolute contrast examples (b) for defect on left side and intact area for the multi-stringer component

(a)　　　　　　　　　　　　　　　　(b)
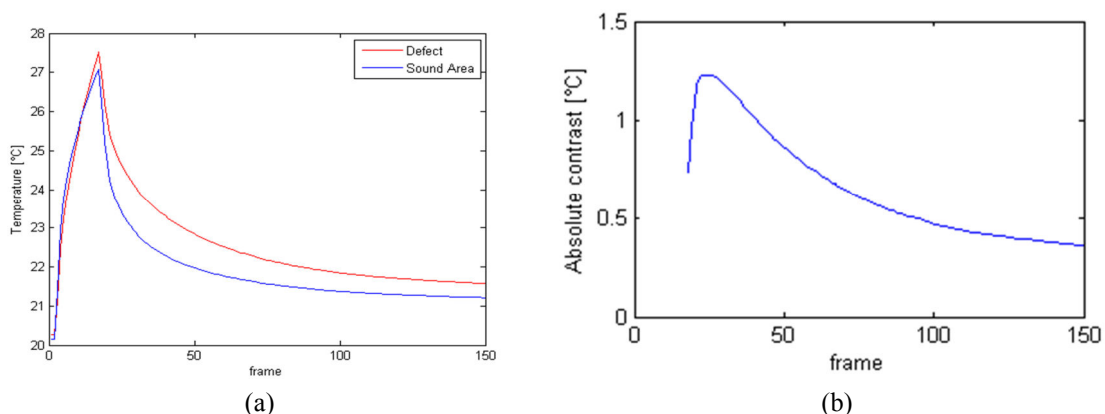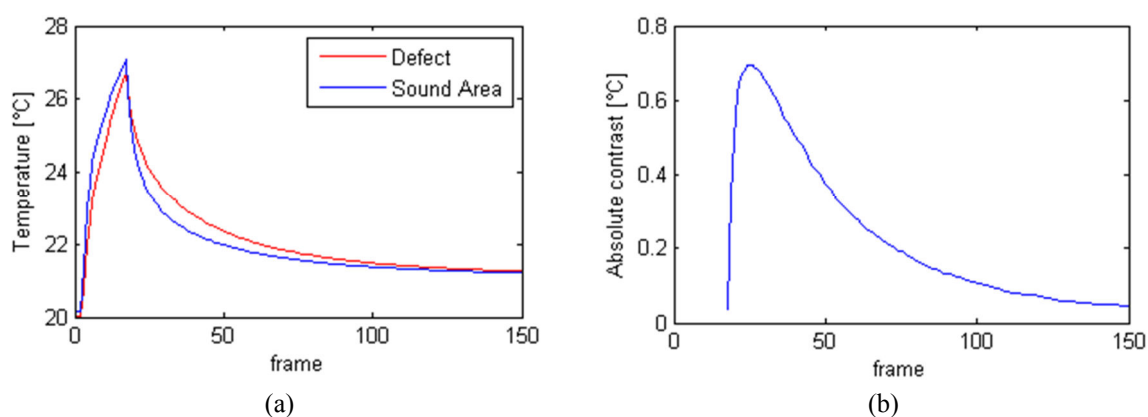
Fig. 11 - Thermal profiles (a) and the Absolute contrast examples (b) for defect on right side and intact area for the multi-stringer component

The following Tables 6 and 7 report the detected maximum values of absolute contrast (Ca_max), as evaluated for the two defects in computation zones for plate-I of different size. The first table shows results for rectangular shape computation zone for intact and defective areas, as seen in Figure 7 (a). The second table compares results for rectangular and circular shape zones, as seen in Figure 12, showing higher contrast values in the case of rectangular shapes with respect to circular shapes for defect 1. These tables show the randomness of data with the operator choice of both shapes and size for both reference intact and damaged area.

Table 6 - Maximum Absolute Contrast Value for rectangular computation shape zone

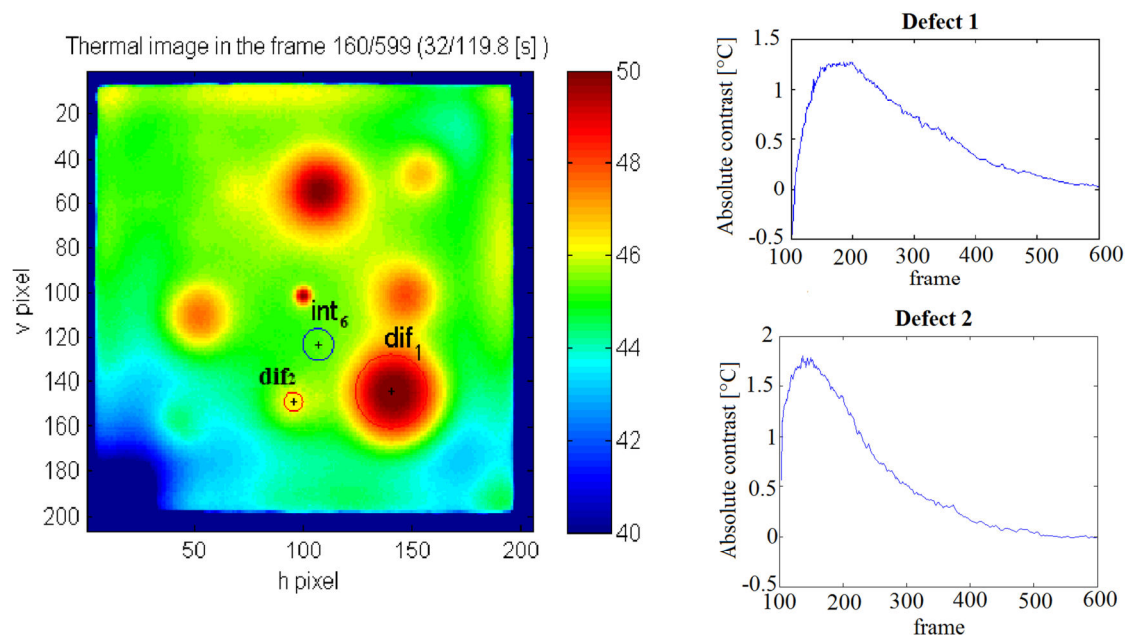| Intact computation zone (px²)	CA_MAX VALUE OF DEFECT 1 [°C]		CA_MAX VALUE OF DEFECT 2 [°C]	
	C_A in Defective computation zone N.° 1 (20 x 30 px²)	C_A in Defective computation zone N.° 2 (10 x 15 px²)	C_A in Defective computation zone N.° 1 (8 x 14 px²)	C_A in Defective computation zone N.° 2 (5 x 10 px²)
14 x 12	4.0222	4.7220	0.8999	0.9935
21 x 30	4.8662	5.5675	1.7359	1.8294
14 x 20	3.7277	4.4331	0.6209	0.7178
19 x 20	3.4096	4.1125	0.3674	0.4614
13 x 20	3.8448	4.5466	0.7502	0.8411
Mean value	3,97	4,68	0,87	2,00
Standard Deviation	0,55	0,55	0,52	0,55

Fig. 12 - Thermal image of plate-I with circular reference zones and defect's relative Absolute contrast examples.

Table 7 - Maximum Absolute Contrast Value for rectangular and circular computation shape zone

CA_MAX VALUE OF DEFECT 1 [°C]				CA_MAX VALUE OF DEFECT 2 [°C]			
Rectangular shape area		Circular shape area		Rectangular shape area		Circular shape area	
Intact zone (px^2)	C_A in Defective area N.° 1 (20 x 30 px^2)	Intact zone (Ø px)	C_A in Defective zone N.° 3 (Ø 33 px)	Intact Zone (px^2)	C_A in Defective zone N.° 1 (8 x 14 px^2)	Intact Zone (Ø px)	C_A in Defective zone N.° 3 (Ø 9 px)
14 x 12	4.0222	14	1.2740	14 x 12	0.8999	14	1.8082
21 x 30	4.8662	30	0.9066	21 x 30	1.7359	30	1.4950
14 x 20	3.7277	20	1.1117	14 x 20	0.6209	20	1.6824
19 x 20	3.4096	16	2.3827	19 x 20	0.3674	16	2.9002
13 x 20	3.8448	18	1.6937	13 x 20	0.7502	18	2.1218
Mean value	3,97		1,47		0,87		2,00
Standard Deviation	0,55		0,58		0,52		0,55

In the tables, we can notice that the intact zone's choice significantly influence the analytical determination of the thermal contrast curve and the consequent evaluation of the Ca_max, used to characterize the defect criticality. From the previous image, sometimes the heating is not uniform on the specimen surface, the defect's size influences the Ca_max and the choice of intact areas is a determining factor in the contrast computation.

Custom field contrast results

The determination of the thermal contrast has two limitations: the assumption to know the reference non-defective zones of specimen and the dependence of the thermal contrast from the choice of the intact and defective zone analysis. Another limitation is that the analysis is

done at the local level and undergoes preliminary choices of the operator on thermograms. Sometimes, the heat quantity deposited by the external source is not uniform, so different zones have different cooling temperatures and gradients and different defects can be misjudged as identical.

SDI method allows us to analyze a single defect at a time: therefore, it was necessary a new algorithm method to be implemented on Matlab and take in account such limitations and improve the thermographic-processing technique, to enhance the inspection of defects in terms of accuracy.

A new contrast algorithm is based on a method with allows defect mapping defined by the value of contrasts, as distributed completely on inspected specimen. Therefore, the method automates the detection and mapping simultaneously of the local contrast to identify defect boundaries onto the whole surface. In other words, the local contrast is automatically determined investigating the zone with highest temperature in pre-defined areas.

For each pixel of the thermographic image, new Matlab procedures rework the differences of the reference temperatures determined in the two-dimensional array of pixels in the proximity of the calculation point. This algorithm is based on the principle for which the reference temperatures evaluated around the chosen inspected spot tend to reach similar values when overpass the defect border, leading to small Local Contrast variations whose values are displayed with zero edges on contrast maps, clearly distinguishing the damaged zones and defect shape. The iterative calculations for all pixels on specimen allow achieving defect representation for the whole specimen. Figure 13 shows a Comparison between original thermal map (a) and the proposed Contrast Image (b) of CFRP plate-I on side B (defects' depth of 2.8 mm) obtained after 11.6 cooling seconds after heating pulse of 20 s.

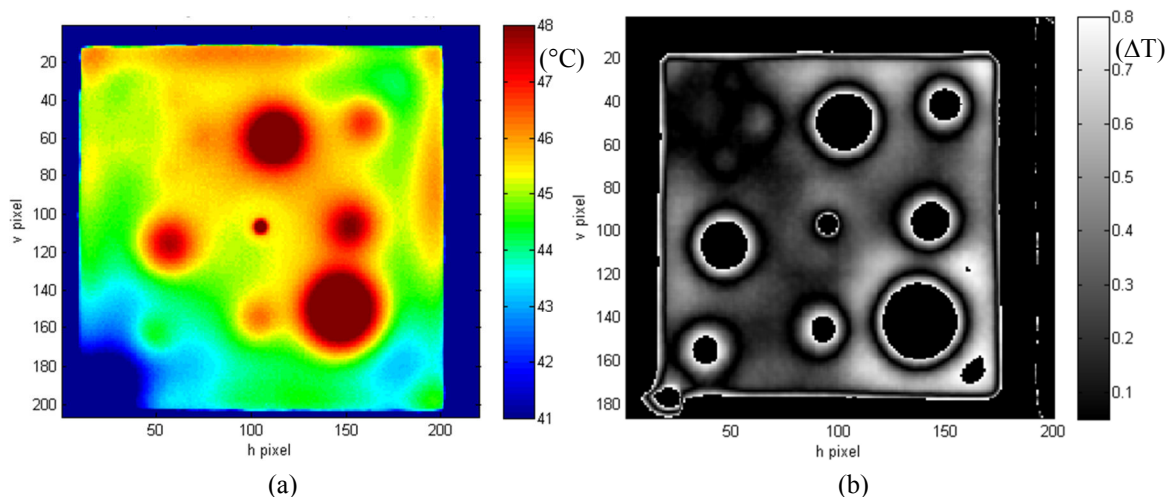(a)   (b)

Fig. 13 - Comparison between Thermal map (a) and Contrast map (b) of CFRP plate-I (side B).

Despite the heating not ideal, the contrasts map allows easily identifying even the smallest defects up to 5 mm of diameter in a single spot (top left). The proposed contrast resulted by local temperature differences allows the evaluation of internal defects and is physically explained by the fact that the thermal properties of defects are different from those of the surrounding material.

Contrast mapping has been optimized in order to highlight the most reliable boundary for the found defects of various types in carbon fibre and glass fibre plates, significantly reducing the background noise effects and possible defective indications.

Figures 14 and 15 other examples of thermal and contrast maps obtained on CFRP plates. In the contrast map of plate-II on side-A (Figure 15(b)), four small defects of 5 mm diameter are clearly distinguished.

The greater depth of defects in the plate-I/ side A (4,9 mm of depth) causes difficulty of plate inspection and therefore we use longest heating times (Table 4). However, higher heating times do not allow smaller defects detection; therefore, it was not possible to identify defects with less than 15 mm diameter. From CFRP plate-II acquisitions, the heating time of 15s allows us to detect more clearly the greatest number of defects.
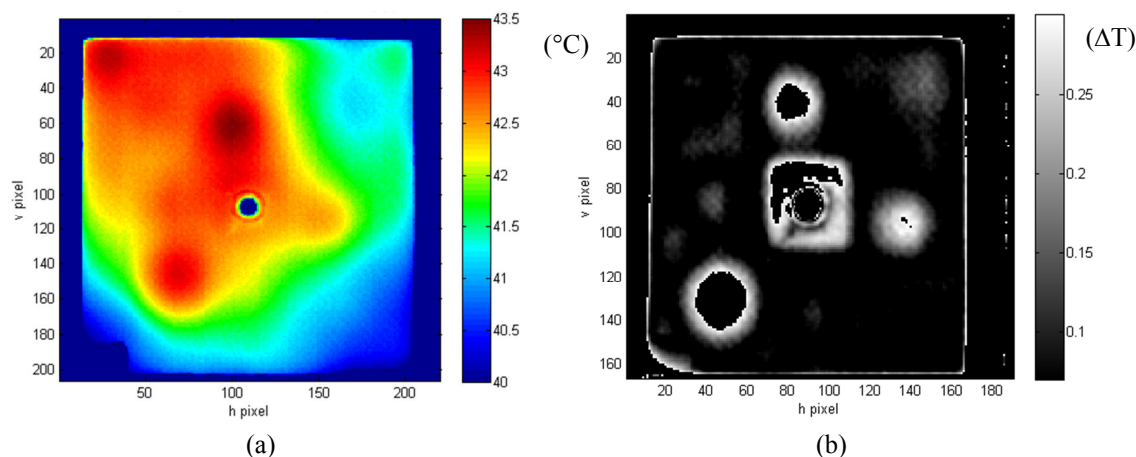

(a)   (b)

Fig. 14 - Comparison between Thermal map (a) and Contrast Image (b) of CFRP plate-I on side A obtained after 39.4 cooling seconds after heating pulse of 30 s.

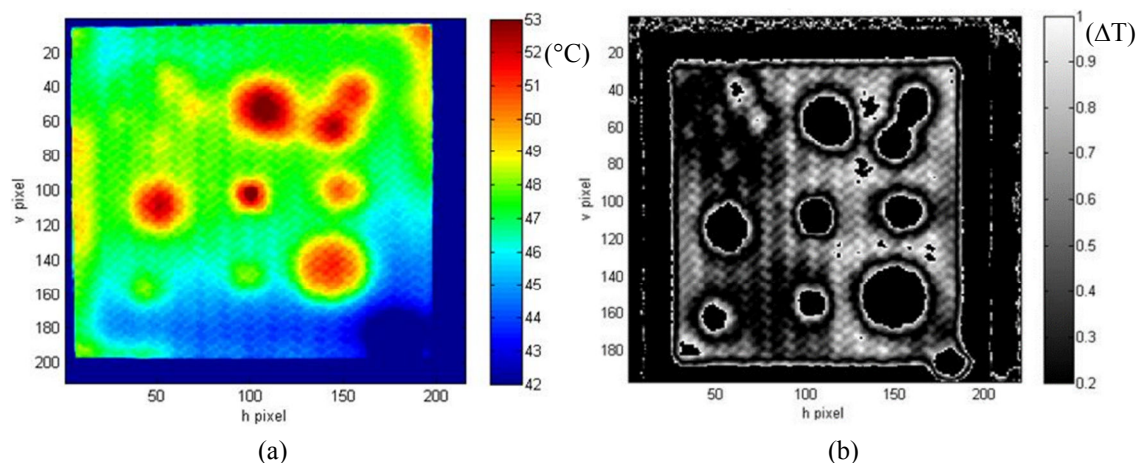(a)   (b)

Fig. 15 - Comparison between Thermal map (a) and Contrast Image (b) of CFRP plate-II on side A obtained after 5 cooling seconds after heating pulse of 15 s.

The authors performed UT inspections for a preliminary evaluation of the damaged areas around central cut under compression load test of the real component. Olympus Omni-scan MXU is the test instrument used, with an innovative technological 64 elements Phased Array (PA) probe.

The Phased Array system uses the physical principle of multiple progressive waves, varying the time between a series of ultrasonic pulses. So the wave front generated by each element of the array at slightly different times combines with other elements pulses to direct and shape the intact beam and achieve a sharp focus and different beam direction (A. P. Carofalo *et al*., 2014).

In the Figure 16, an example of ultrasonic control with the Phased Array technology is showed around the central damaged zones; the ultrasonic local sectional scans showed the presence of widespread defective areas around the cut extremities.

In Figure 17 there is the whole C-scan mapping of the damaged area, in the functional direction along the simulated impacted zone, where is clearly highlighted the delamination zones' extension.
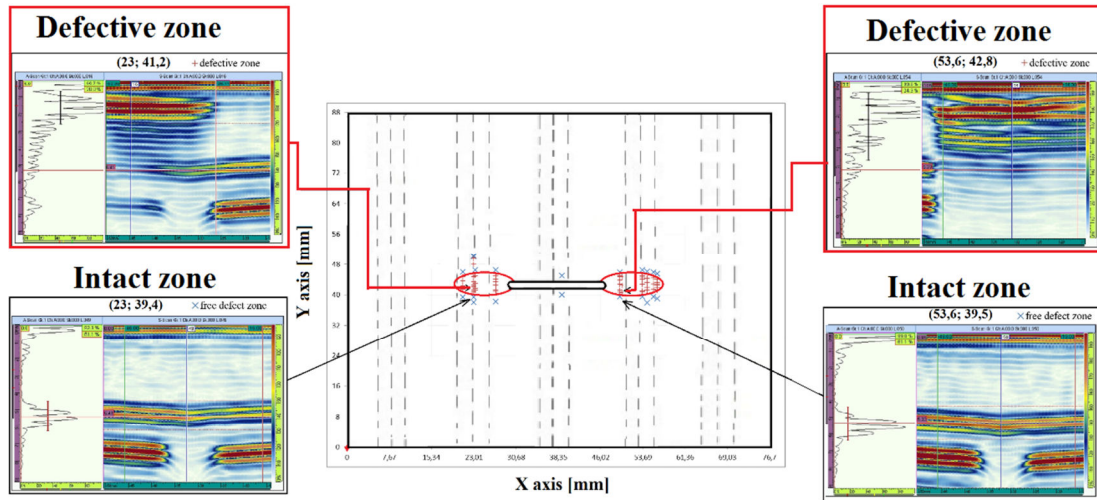

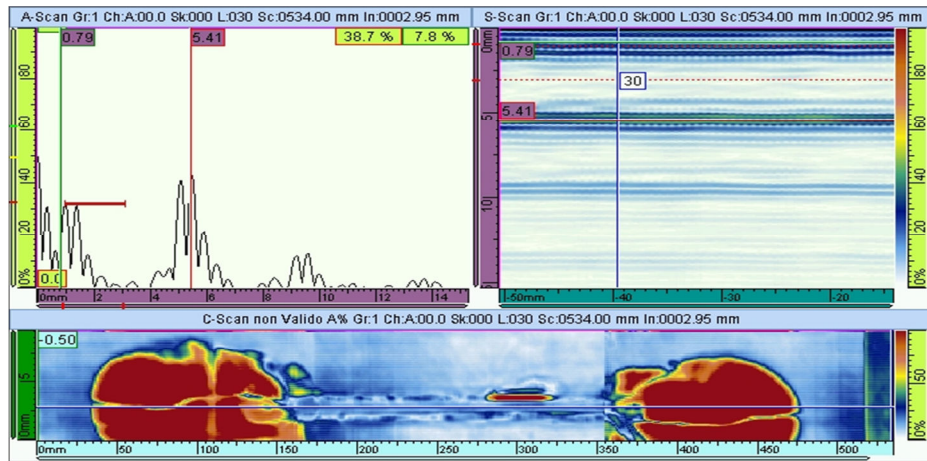Fig. 16 - Ultrasonic inspection over the multi-stringer component' surface.

Fig. 17 - C-scan inspection over the multi-stringer component' surface on damaged zone along the artificial cut.

The thermal acquisitions of aeronautical component are successively focused on impact damage area in order to identify data correlation with UT controls. Several acquisitions described in the table 5 were carried out for the aeronautical component and with heating time of 3s and 7s are shown in Figures 17(a) and 17(b) respectively, as an example.

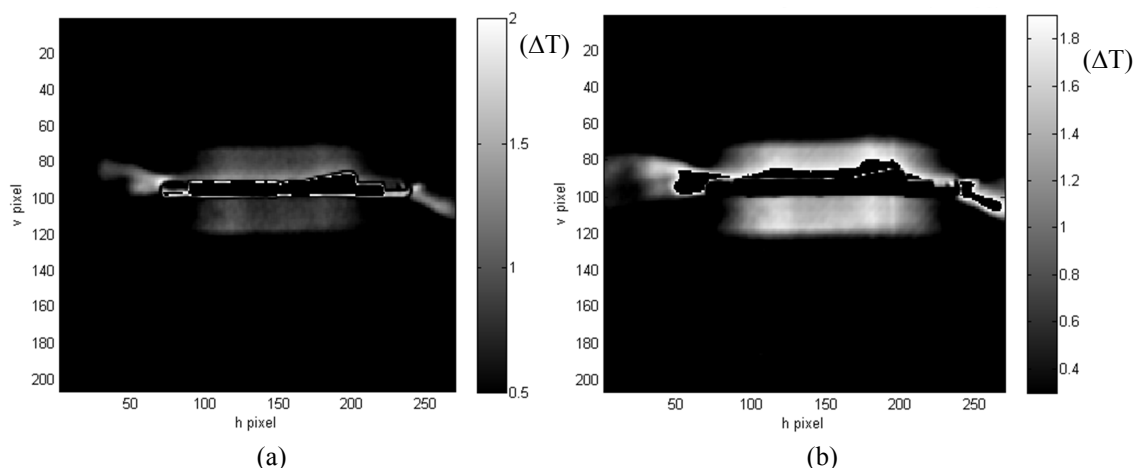(a)   (b)

Fig. 17 -Contrast map of multi-stringer component using heating pulse of 3s (a) and using heating pulse of 7s.

Thermal results are conform to obtained ultrasonic inspections, but in this case, the local contrast map seem to under estimate the defect extension with respect to UT results. This is due to the need to calibrate the method algorithm on the specimen sizes and materials.

Finally, the matlab scripts were refined to create contrast maps without the false defective indications, which are sometimes present in the previous maps, and to improve the contours of the standard defects. The development of the new algorithms improves thermographic analysis procedure for detection and quantification of dimensional FRP bonding defects. Figure 18 shows a comparison example between different Contrast maps obtained with new matlab scripts, modifying the algorithm equations.

ORIGINAL CONTRAST   OPTION A   OPTION B
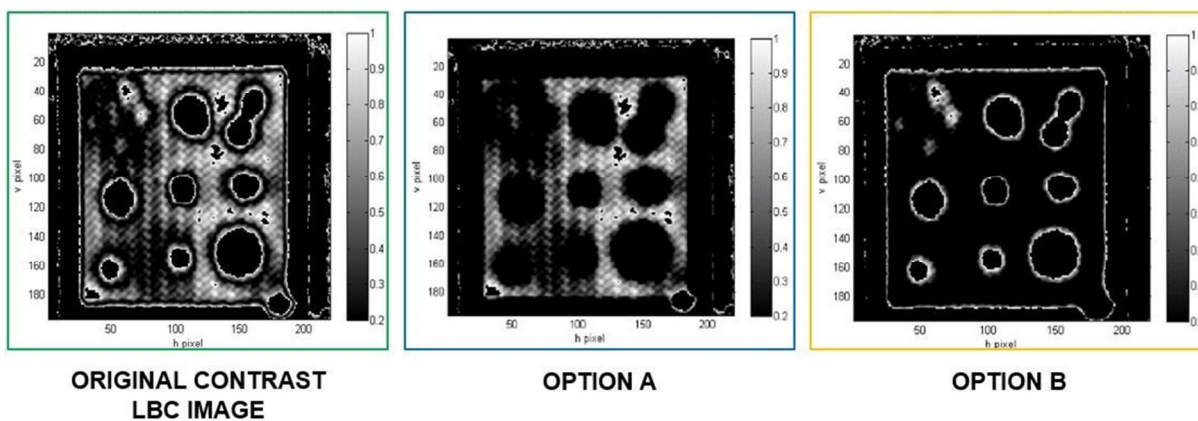LBC IMAGE

Fig. 18 - Comparison between different Contrast maps of CFRP plate-II on side-A, with modified scripts.

CONCLUSIONS

The contrast maps allow highlighting all the defects displayed in the corresponding thermal maps; the larger defects' diameters are more noticeable than others, either on side A or 6 layers side and on either side B or 8 layers side on both type of specimens. The depth at which the defects are located determines the thermographic visibility of the smaller ones. Obviously, the defects observed in the side A are more easily identifiable and are greater in number than those on the two side B because the side A has a lower thickness than the other ones.

The new contrast pattern allows us to visualize the defects edge, with a dependency on the depth and thickness of the defect itself, but there are limitations. In fact, the definition of the image and the optical focus do not depend on the algorithm, but from the choice of thermal camera and set-up for the acquisitions.

REFERENCES

[1] Dattoma V., S. Giancane, F. Palano, F.W. Panella, "ND small defects detection of GFRP laminates using pulsed thermography", Structural Integrity and Life, Vol. 12, No 2 (2012), pp. 109-116.

[2] Carofalo, A., V. Dattoma, F.W. Panella, F. Palano, and S. Giancane. 2012. "Rilevazione di difetti in compositi GFRP mediante termografia pulsata e lock-in." AIAS - Associazione Italiana per L'Analise delle Sollecitazioni 41° Convegno Nazionale, 5-8 Settembre 2012, Università Degli Studi di Padova, August 9, 2012, sec. Università del Salento - Dipartimento di Ingegneria dell'Innovazione.

[3] Carofalo, A. P., V. Dattoma, F. Palano, and F. W. Panella. 2014. "ND Testing Advances on CFRP with Ultrasonic and Thermal Techniques, 16th European Conference on Composite Materials ECCM 16, Seville (Spain)," June 22, 2014.

[4] Czichos, Horst. 2013. Handbook of Technical Diagnostics: Fundamentals and Application to Structures and Systems. Springer Science & Business Media.

[5] Dattoma, V., R. Nobile, F. W. Panella, and A. Saponaro. 2017. "NDT Thermographic Techniques on CFRP Structural Components for Aeronautical Application," Proceeding of 46° National Congress, Pisa (Italy).," June 9, 2017.

[6] Gholizadeh, S. 2016. "A Review of Non-Destructive Testing Methods of Composite Materials." Procedia Structural Integrity, XV Portuguese Conference on Fracture, PCF 2016, 10-12 February 2016, Paco de Arcos, Portugal, 1 (January):50-57. https://doi.org/10.1016/j.prostr.2016.02.008.

[7] Susa, M., X. Maldague, and I. Boras. 2010. "Improved Method for Absolute Thermal Contrast Evaluation Using Source Distribution Image (SDI)." Infrared Physics & Technology 53 (3):197-203. https://doi.org/10.1016/j.infrared.2009.11.008.